Effect of Fluid-Solid Interactions on Symmetry Breaking in Closed Nanoslits

Gersh O. Berim and Eli Ruckenstein*

Department of Chemical and Biological Engineering, State University of New York at Buffalo, Buffalo, New York 14260

Received: February 28, 2007; In Final Form: August 1, 2007

The possibility of symmetry breaking of the fluid (argon) density distribution across a long closed slit with identical walls composed of solid carbon dioxide was noted in previous papers by the authors. The main conclusion was that there is a range of average densities in which symmetry breaking occurs and that outside that range the fluid density profile is symmetrical. A critical temperature T_{sb} was also identified below which symmetry breaking can occur. In this paper, symmetry breaking is examined for walls made of other materials and it is shown that it occurs only when the energy parameter ϵ_{fw} of the fluid−wall interaction in the Lennard-Jones potential satisfies the inequalities $\epsilon_{fw1} \leq \epsilon_{fw} \leq \epsilon_{fw2}$, where ϵ_{fw1} and ϵ_{fw2} are temperature-dependent critical values of ϵ_{fw}. The value of ϵ_{fw1} increases and that of ϵ_{fw2} decreases with increasing temperature. The comparison of the theory with Monte Carlo simulations confirms the existence of symmetry breaking across the slit. The possibility of symmetry breaking along the slit is also noted.

1. Introduction

A fluid in a slit with identical walls is subjected to an external potential due to the fluid−solid interactions which possess a reflectional symmetry about the middle of the slit. The same symmetry is present in the basic Euler−Lagrange equation,[1] which describes the equilibrium density profile across the slit and provides a symmetrical solution for the profile.[1−7] However, it is known that in some cases the symmetry of the stable state of a system can be lower than the symmetry of the equations describing the system. This symmetry breaking (SB) is well-known in physics, chemistry, biology, etc. A classical example from the physics of fluids is the freezing transition[8] in which the continuous translational symmetry of a fluid (in the absence of an external potential) is broken. The discrete symmetry, e.g., reflectional, or the left−right one, can also be broken. A well-known example is the occurrence of spontaneous magnetization in ferromagnetic materials in the absence of an external magnetic field at temperatures lower than the Curie temperature. The possibility of a reflectional SB was demonstrated in ref 9 for an open system consisting of two parallel identical layers of a two-dimensional liquid coupled by an interlayer potential.

In ref 10, the existence of SB for fluid density profiles across a long closed nanoslit with identical walls was predicted by employing the local density functional theory (DFT) and was confirmed later in ref 11 with a more accurate nonlocal DFT. Argon was the fluid, and the walls were considered composed of carbon dioxide. Lennard-Jones potentials were used for both the fluid−fluid and fluid-walls interactions. It was shown that, for selected values of the energy parameters of the fluid−fluid (ϵ_{ff}) and fluid−walls (ϵ_{fw}) interactions, the Euler−Lagrange equation for the fluid density profile has in some cases two solutions. One of them is symmetrical about the middle of the slit and the other one asymmetrical. The free energy of the state described by the asymmetrical profile was always lower than for the symmetrical profile. Therefore, the stable state of the system is that with the asymmetrical density distribution across the slit, and the state possessing a symmetrical density distribution is metastable. Such a symmetry breaking occurred only in some domain of the $\rho_{av}-T$ plane, where ρ_{av} and T are the average fluid density in the slit and the absolute temperature, respectively. In the present paper, the considerations of ref 11 are extended to other wall materials which are characterized by the fluid-wall energy parameter ϵ_{fw}. It is shown that there are two temperature-dependent critical values of ϵ_{fw}, ϵ_{fw1} and ϵ_{fw2}, and that SB occurs when ϵ_{fw} is between those two critical values. In addition, in the last section, we compare some of our results with Monte Carlo simulations.

2. Background

The system under consideration was described in detail in ref 11. It consists of one component fluid (argon) confined in a long closed nanoslit between two parallel structureless identical solid walls W_1 and W_2 separated by a distance L (see Figure 1). The distance between the side walls which close the slit is considered to be very large compared to L. As a result, the end effects can be considered negligible. It is also assumed that the density distribution is a function of only a single coordinate h (see Figure 1) that represents the distance of the fluid molecules from the left wall. The closed slit with planar walls can be also imagined as a thin layer of thickness L between a solid cylinder of large radius R ($R \rightarrow \infty$) embedded into a cylindrical cavity of radius $R + L$.

The interaction between fluid molecules is considered as the sum of a potential energy of a reference system (hard spheres) and an attractive perturbation which is treated in the mean-field approximation.

The attractive part of the fluid−fluid interactions is described by the Lennard-Jones 6−12 potential, $\phi_{ff}(|\mathbf{r} - \mathbf{r}'|) = 4\epsilon_{ff}[(\sigma_{ff}/r)^{12} - (\sigma_{ff}/r)^6]$ for $r \geq \sigma_{ff}$ ($r = |\mathbf{r} - \mathbf{r}'|$) and $\phi_{ff}(|\mathbf{r} - \mathbf{r}'|) = 0$ for $r < \sigma_{ff}$. The interaction between the molecules of the fluid and those of the walls are described by the potential $\phi_{fw}(|\mathbf{r} - \mathbf{r}'|) = 4\epsilon_{fw}[(\sigma_{fw}/r)^{12} - (\sigma_{fw}/r)^6]$ for $r \geq \sigma_{fw}$ and $\phi_{fw}(|\mathbf{r} - \mathbf{r}'|) =$

* Author to whom correspondence should be addressed. E-mail: feaeliru@acsu.buffalo.edu. Phone: (716) 645−2911, ext. 2214. Fax: (716) 645−3822.

10.1021/jp071667b CCC: $37.00
Published on Web 10/19/2007

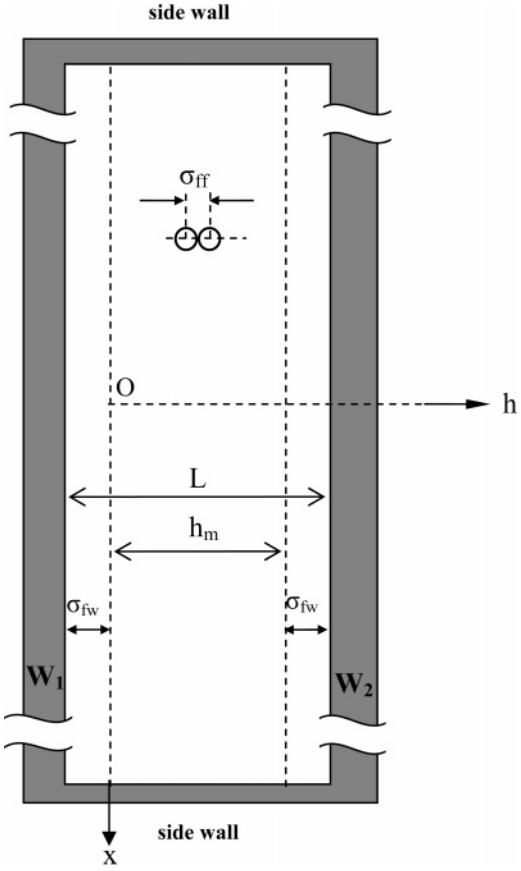

Figure 1. Closed slit of width L between two identical solid walls W_1 and W_2. σ_{ff} and σ_{fw} are the hard core diameters of the fluid−fluid and fluid−wall interactions, respectively. The y axis is perpendicular to the plane of the figure.

∞ for $r < \sigma_{fw}$. In the above potentials, σ_{ff} and σ_{fw} are hard core diameters and ϵ_{ff} and ϵ_{fw} are interaction energy parameters for fluid−fluid and fluid-walls interactions, respectively. The vectors $\mathbf{r}$ and $\mathbf{r}'$ provide the positions of the interacting molecules.

The density distribution of the fluid in the slit will be calculated using a nonlocal density functional theory of the form presented in ref 1. Such a theory was successfully used to describe a fluid in an open slit,[1,6,7,12] both for small and large fluid densities.

The Helmholtz free energy F of a system is given by

$$F = \int_0^{h_m} \mathrm{d}h \left[k_B T \rho \,[\log(\Lambda^3\rho) - 1] + \rho \Delta\Psi_{hs}(h) + \frac{1}{2}\rho U_f(h) + \rho U_s(h) \right] \quad (1)$$

where $\rho \equiv \rho(h)$ is the density profile, $\Lambda = h_P/(2\pi m k_B T)^{1/2}$ is the thermal de Broglie wavelength, h_P and k_B are the Planck and Boltzmann constants, respectively, m is the mass of a fluid molecule, T is the absolute temperature, $h_m = L - 2\sigma_{fw}$ (see Figure 1). The function $\rho\Delta\Psi_{hs}(h)$ represents the free energy density of a hard core fluid and has the form

$$\rho \Delta\Psi_{hs}(h) = k_B T \rho \eta_{\bar\rho} \frac{4 - 3\eta_{\bar\rho}}{(1 - \eta_{\bar\rho})^2} \quad (2)$$

where $\eta_{\bar\rho} = (1/6)\pi\bar\rho(h)\sigma_{ff}^3$ is the packing fraction of the fluid molecules and $\bar\rho(h)$ is the smoothed density. The functions $U_f(h)$ and $U_s(h)$ account for the interactions between the fluid molecules and the fluid molecules with the solid walls, respectively. Their explicit expressions are provided in Appendix A. Here and below all extensive quantities (free energy, number of molecules N, volume V) are expressed per unit area of one wall.

The Euler−Lagrange equation for the density profile ρ in a closed slit, obtained by minimizing F, has the following form:[11]

$$k_B T \log(\Lambda^3\rho) + \Delta\Psi_{hs}(h) + \overline{\Delta\Psi'}_{hs}(h) + U_f(h) + U_s(h) = \lambda \quad (3)$$

where λ is the Lagrange multiplier arising because of the constraint

$$N = \int_0^{h_m} \rho(h)\, \mathrm{d}h \quad (4)$$

of constant number of molecules in the closed slit and

$$\overline{\Delta\Psi'}_{hs}(h) = \sum_{n=0}^{2} \int_V \mathrm{d}\mathbf{r}' \frac{\rho(h') w_n(|\mathbf{r} - \mathbf{r}'|)[\bar\rho(h')]^n}{1 - \bar\rho_1(h') - 2\bar\rho(h')\bar\rho_2(h')} \frac{\partial\Delta\Psi_{hs}[\bar\rho(h')]}{\partial\bar\rho(h')} \quad (5)$$

In eqs 2 and 5

$$\bar\rho(h) = \int_V \mathrm{d}\mathbf{r}'\, \rho(h') w[|\mathbf{r} - \mathbf{r}'|;\, \bar\rho(h)] \quad (6)$$

the weighting functions $w[|\mathbf{r} - \mathbf{r}'|;\, \bar\rho(h)]$ and $w_n(|\mathbf{r} - \mathbf{r}'|)$ and the coefficients $\bar\rho_n(h')$ ($n = 0, 1, 2$) have been taken from refs 1 and 13, and an expression for $(\partial\Delta\Psi_{hs}[\bar\rho(h')]/\partial\bar\rho(h'))$ is provided in Appendix A.

Formally, eq 3 coincides with that for an open system without side walls. However, the Lagrange multiplier λ in closed systems is not known in advance, in contrast to the open systems where λ is the chemical potential. The relation between λ and the number N of molecules is provided by the constraint eq 4 and has the form[11]

$$\lambda = -k_B T \log\left[\frac{1}{N\Lambda^3} \int_0^{h_m} \mathrm{d}h\, \mathrm{e}^{Q(h)}\right] \quad (7)$$

where

$$Q(h) = -\frac{1}{k_B T}[\Delta\Psi_{hs}(h) + \overline{\Delta\Psi'}_{hs}(h) + U_f(h) + U_s(h)] \quad (8)$$

By eliminating λ between eqs 3 and 7, one obtains an integral equation for the density profile $\rho(h)$ that can be solved by numerical iterations of the kind used in ref 13. The input density profile $\rho_i^{in}(h)$ for the $(i + 1)$th iteration $\rho_{i+1}(h)$ generated by the Euler−Lagrange equation is given by the expression

$$\rho_i^{in}(h) = (1 - x)\rho_{i-1}^{in}(h) + x\rho_i(h) \quad (9)$$

where $\rho_i(h)$ is the ith iteration and the constant x was taken 0.01. The value of λ, if needed, can be found from eq 7 using the obtained equilibrium density profile. Owing to the mentioned identity of the Euler−Lagrange equations for $\rho(h)$ in open and closed systems, one can consider the obtained value of λ as the chemical potential of a fictitious open system which has the same density profile as the closed one. (Note, that the state of the open system with such a profile was metastable in all cases considered by us.[11])

For any selected set of parameters (temperature, average density of the fluid in the slit, and strength of the fluid-wall interaction), two initial guesses for the density profile were employed. A homogeneous density equal to a selected average

density was employed as the first initial guess. In this case, the resulting profile was always symmetrical. As a second choice of the initial guess, an asymmetrical profile describing the state with most of the molecules located in the left (right) half of the slit was used. Starting with such a guess, either a symmetrical density profile that coincided with that obtained with the symmetrical initial guess, or an asymmetrical profile representing an additional solution to the Euler−Lagrange equation was obtained. When an asymmetrical density profile was obtained, it always provided a lower free energy than the symmetrical profile.

Let us make some remarks regarding the number of iterations in the numerical computations. As a measure of the precision of the iteration procedure, the dimensionless quantity $\delta = \sigma_{ff}^5 \int_0^{h_m} dh[\rho_{i+1}(h) - \rho_i^{in}(h)]^2$ is introduced which characterizes the difference between $(i + 1)$th iteration $\rho_{i+1}(h)$ and the input profile $\rho_i^{in}(h)$ from which that iteration was obtained. When the initial guess in computations was selected to be homogeneous, the iterations were carried out until δ became smaller than $\epsilon = 10^{-7}$. The increase in precision did not lead to appreciable changes in the density profile. However, during the computation which started with an asymmetrical initial guess, the precision $\epsilon = 10^{-7}$ was not sufficient, because the profile $\rho_i(h)$ which was asymmetrical for $\epsilon = 10^{-7}$ sometimes became symmetrical with increased precision. To increase the confidence that the density profile obtained is symmetrical or asymmetrical, the precision of calculations was increased up to $\epsilon = 10^{-12}$ and the dependence of the parameter

$$\Delta_N = \frac{1}{2N}\int_0^{h_m} dh\, |\rho(h) - \rho(h_m - h)| \qquad (10)$$

on ϵ was examined by varying ϵ from 10^{-7} to 10^{-12}. The parameter Δ_N should be equal to zero if the profile is symmetrical about the middle of the slit and $0 < \Delta_N \leq 1$ in the asymmetrical case. The dependence of Δ_N on ϵ had one of the following two asymptotic behaviors. In the first case, Δ_N continuously decreased approaching zero. The resulting profile in this case was considered symmetrical even though the profile obtained after achiving the precision $\epsilon = 10^{-12}$ had a small asymmetry. In the second case, Δ_N reached a nonzero asymptotic value beginning with some $\epsilon > 10^{-12}$ (say, $\epsilon = 10^{-9}$), which remained unchanged with increasing precision. Only in such a case the resulting asymmetric profile was considered to be a solution of the Euler−Lagrange equation.

All obtained density profiles were tested with respect to their thermodynamic stability by examining their response to arbitrarily small perturbations of the density distribution. To perform such a test we used the second variation δ^2F of the free energy F with respect to the fluid density profile, which has the following general form

$$\delta^2F = \int_0^{h_m} dh\, \delta\rho(h) \int_0^{h_m} dh'\, X(h,h')\delta\rho(h') \qquad (11)$$

where $\delta\rho(h)$ is a small perturbation of the density profile and $X(h, h')$ is a function of $\rho(h)$ and $\rho(h')$. The explicit form of $X(h, h')$ is provided in Appendix B. The state of the system described by a given density profile is stable if δ^2F is positive for any $\delta\rho(h)$. In this case, the free energy of the system has a local minimum for that profile. Because the interactions depend on the densities in two different points, it is difficult to provide a general proof of the stability condition. Instead, we checked the sign of δ^2F for a variety of small perturbations. For example, perturbations of the form

$$\delta\rho(h) = A(h) + B(h)\left[\sin\left(\frac{2\pi h}{h_m}n_1\right)\right]^{n_2} + C(h)\left[\cos\left(\frac{2\pi h}{h_m}n_3\right)\right]^{n_4} \qquad (12)$$

were considered, where $A(h)$, $B(h)$, and $C(h)$ have the form of power or exponential functions of h and n_1, ..., n_4 are constants (not neccessarly integers). The coefficients have been adjusted to maintain the number of molecules in the slit constant. In all considered cases, the second variation was positive, confirming the thermodynamic stability of the obtained density profiles.

3. Results

In the calculations, the parameters ϵ_{ff} and σ_{ff} were selected as for argon:[14] $\epsilon_{ff}/k_B = 119.76$ K, $\sigma_{ff} = 3.405$ Å. The chemical nature of the walls was taken into account only through the energy parameter ϵ_{fw}, whereas the hard core diameter σ_{fw} and the walls density ρ_w were kept constant, $\sigma_{fw} = 3.727$ Å, $\rho_w = 1.91 \times 10^{28}$ m^{-3}. The width of the slit was taken $h_m = 15\sigma_{ff}$. The dimensionless quantities $\rho^* = \rho\sigma_{ff}^3$, $h^* = h/\sigma_{ff}$ for the fluid density and distance from the wall, respectively, were employed in the calculations. In what follows, ϵ_{fw} will be expressed in units of the energy parameter ϵ_{ff} through the dimensionless quantity $\varepsilon_{fw} = \epsilon_{fw}/\epsilon_{ff}$.

In ref 11, it was shown that at a selected temperature $T < T_{sb}$, where T_{sb} is a critical temperature above which no symmetry breaking occurs, SB was observed only for an average fluid density $\rho_{av}^* = N\sigma_{ff}^2/h_m^*$ in the slit which satisfies the inequalities $\rho_{sb1}^* < \rho_{av}^* < \rho_{sb2}^*$, where the critical densities ρ_{sb1}^* and ρ_{sb2}^* depend on temperature. For instance, for $\varepsilon_{fw} = 1.277$ (walls of solid carbon dioxide) and $T = 104$ K, $\rho_{sb1}^* = 0.1971$ and $\rho_{sb2}^* = 0.3517$.[11] As expected, the present calculations show that at a selected temperature the critical values ρ_{sb1}^* and ρ_{sb2}^* depend also on ε_{fw}. In Figure 2a, the dependencies of ρ_{sb1}^* and ρ_{sb2}^* on ε_{fw} are plotted for $T = 104$ K. Symmetry breaking occurs only for those $\rho_{av}^* - \varepsilon_{fw}$ pairs which are located inside the area *ABCD*. For $\varepsilon_{fw} < \varepsilon_{fw1}$ or $\varepsilon_{fw} > \varepsilon_{fw2}$, where $\varepsilon_{fw1} = 0.34$ and $\varepsilon_{fw2} = 1.38$ are critical values, no SB occurs and the density profile is symmetric.

The dependence on ε_{fw} of the difference $\Delta\rho_{av}^* = \rho_{sb2}^* - \rho_{sb1}^*$ between the average critical densities in which SB occurs is presented in Figure 2b which shows that $\Delta\rho_{av}^*$ passses through a maximum $\Delta\rho_{av}^* = 0.1855$ at $\varepsilon_{fw} = 0.986$. In the latter case, $\rho_{sb1}^* = 0.1662$ and $\rho_{sb2}^* = 0.3517$.

As shown in Figure 3, the critical values ε_{fw1} and ε_{fw2} depend on temperature. The former slightly increases and the latter decreases with increasing temperature. As a result, the interval $\Delta\varepsilon_{fw} = \varepsilon_{fw2} - \varepsilon_{fw1}$ in which SB occurs decreases with increasing temperature.

By increasing the average fluid density ρ_{av}^* at a fixed value of ε_{fw}, the density profile of the stable state of the system first looses its symmetry for ρ_{av}^* larger than ρ_{sb1}^* and then restores it for ρ_{av}^* larger than ρ_{sb2}^*. In Figure 4a, the stable profiles corresponding to $\rho_{av}^* = 0.1005$, 0.1546, and 0.3092 are presented for $T = 87$ K and $\varepsilon_{fw} = 0.639$. (At that temperature, $\rho_{sb1}^* = 0.1051$, and $\rho_{sb2}^* = 0.5241$). For $\rho_{av}^* = 0.1005$ the profile is symmetrical and for $\rho_{av}^* = 0.1546$ and $\rho_{av}^* = 0.3092$ they are asymmetrical. The restoring of the profile symmetry near ρ_{sb2}^* is illustrated in Figure 4b where the profiles for $\rho_{av}^* = 0.5194$, 0.5225 (asymmetrical), and 0.5411 (symmetrical) are presented. Note that, in addition to an asymmetrical density profile, the Euler−Lagrange equation for the same set of parameters

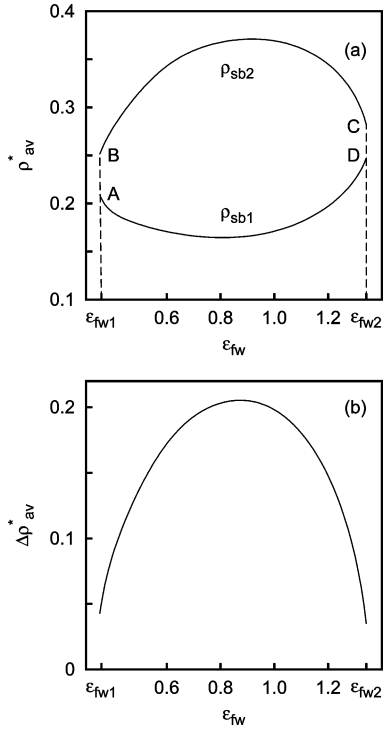

Figure 2. (a) Dependence of the critical densities ρ^*_{sb1} and ρ^*_{sb2} on ε_{fw} for $T = 104$ K. Symmetry breaking occurs only for those $(\rho^*_{av} - \varepsilon_{fw})$ pairs which are inside the area *ABCD*. The critical values of ε_{fw} are equal to $\varepsilon_{fw1} = 0.34$ and $\varepsilon_{fw2} = 1.38$. (b) Dependence of the interval $\Delta\rho^*_{av} = \rho^*_{sb2} - \rho^*_{sb1}$ on ε_{fw} for $T = 104$ K.

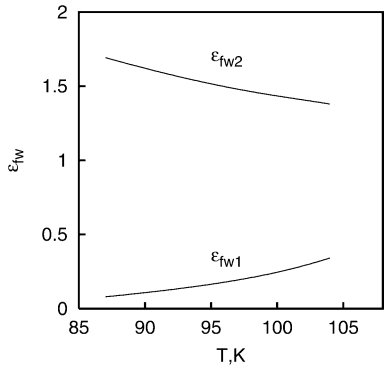

Figure 3. Temperature dependence of the critical values ε_{fw1} and ε_{fw2}. At fixed temperature, symmetry breaking occurs only if $\varepsilon_{fw1} < \varepsilon_{fw} < \varepsilon_{fw2}$.

provides also a symmetrical profile which has, however, a higher free energy than the asymmetrical one. For illustration, the free energies of the asymmetrical profiles of Figure 4a,b are presented in Table 1 along with the free energies of the related symmetrical profiles.

At fixed values of ρ^*_{av} and T the shape of the stable profile depends on ε_{fw}. As an example, the profiles for $\rho^*_{av} = 0.2319$ and $\varepsilon_{fw} = 0.013$, 0.639, 1.534, and 1.789 are plotted in Figure 5 for $T = 87$ K. In this case, SB occurs for $0.08 < \varepsilon_{fw} < 1.693$. Consequently, the profiles plotted for $\varepsilon_{fw} = 0.013$ and $\varepsilon_{fw} = 1.789$ are symmetrical and those for $\varepsilon_{fw} = 0.639$ and $\varepsilon_{fw} = 1.534$ asymmetrical. For the smallest value of $\varepsilon_{fw} = 0.013$, the fluid density near the walls is gas-like $[\rho^*(0) = \rho^*(h_m) \simeq 0.022]$ and in the middle of the slit it is liquid-like $[\rho^*(h_m/2) \simeq 0.58]$. Owing to the weak fluid-wall interactions, there are no visible density oscillations near the walls. For the largest value $\varepsilon_{fw} = 1.4$, the stable density profile is also symmetrical. The fluid density has the largest value at the walls $[\rho^*(0) = \rho^*(h_m) \simeq$ 4.46] and the smallest at the middle of the slit $[\rho^*(h_m/2) \simeq 0.021]$. There are density oscillations near the walls which have a large amplitude and penetrate into the slit up to two molecular diameters. The fluid density in the asymmetrical profiles has the largest, liquid-like, value near the left wall, which increases with increasing ε_{fw}. The depth of penetration of the oscillations into the slit increases with ε_{fw} and for $\varepsilon_{fw} = 1.534$ becomes about four molecular diameters.

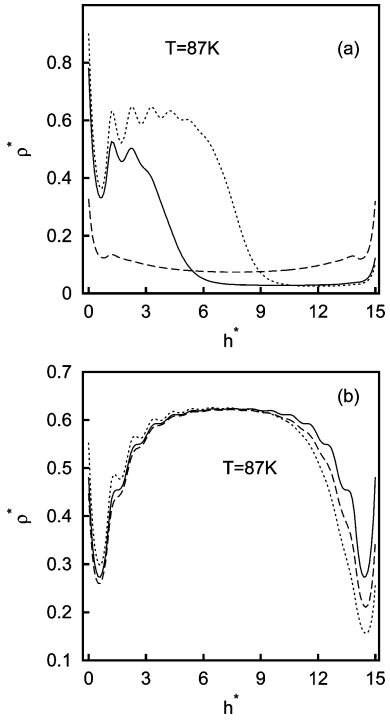

Figure 4. Stable density profiles for $\varepsilon_{fw} = 0.639$ and $T = 87$ K. In this case $\rho^*_{sb1} = 0.1051$, $\rho^*_{sb2} = 0.5241$. (a) Profiles for $\rho^*_{av} = 0.1005$ (dashed line), 0.1546 (solid line), and 0.3092 (dotted line). The first one is symmetrical about the middle of the slit, whereas the other two are asymmetrical. (b) Profiles for $\rho^*_{av} = 0.5194$ (dotted line), 0.5225 (dashed line), and 0.5411 (solid line). The last profile is symmetrical about the middle of the slit, the other two are asymmetrical.

TABLE 1: Values (per Unit Area of One Wall) of the Helmholtz Free Energies F_{sym} and F_{asym} of the Metastable (Symmetric Density Profile) and Stable (Asymmetric Density Profile) States of the Fluid in a Slit with $h^*_m = 15$, Respectively, for Various Average Densities $\rho^*_{av1} < \rho^*_{av} < \rho^*_{av2}$[a]

ρ^*_{av}	F_{sym}	F_{asym}
0.1546	−25.76	−25.98
0.3092	−52.06	−52.26
0.5194	−88.21	−88.22
0.5225	−88.75	−88.76

[a] The temperature $T = 87$ K and $\varepsilon_{fw} = 0.639$. The free energies are given in k_BT/σ_{ff}^2 units.

4. Discussion

As shown in previous papers,[10,11] the symmetry breaking of the fluid density profile across a closed slit with identical walls has several critical-like features. First, SB occurs only if the temperature T is smaller than a critical temperature T_{sb} which for argon between solid carbon dioxide walls is equal to $T_{sb} \simeq 106$ K. Second, at selected $T < T_{sb}$, SB occurs only for those fluid average densities ρ_{av} in the slit that are between two critical values, ρ_{av1} and ρ_{av2} $(\rho_{av1} < \rho_{av2})$. Both ρ_{av1} and ρ_{av2} are temperature dependent.

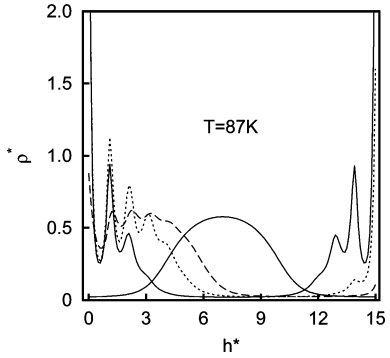

Figure 5. Stable density profiles for $\rho^*_{av} = 0.2319$, $T = 87$ K and various values of ε_{fw}. The symmetrical profiles (solid lines) are for $\varepsilon_{fw} = 0.013$ (has a maximum in the middle of the slit) and $\varepsilon_{fw} = 1.789$. The asymmetrical profiles are for $\varepsilon_{fw} = 0.639$ (dashed line) and $\varepsilon_{fw} = 1.534$ (dotted line). The critical values of ε_{fw} for $\rho^*_{av} = 0.2319$, and $T = 87$ K are $\varepsilon_{fw1} = 0.080$ and $\varepsilon_{fw2} = 1.693$.

In the present paper, one more critical-like feature of SB in a slit was noted. It was shown that, at a selected temperature, SB occurs only if the strength ϵ_{fw} of the fluid−wall interaction is located between two critical values ϵ_{fw1} and ϵ_{fw2}. The value of ϵ_{fw} ($\epsilon_{fw1} < \epsilon_{fw} < \epsilon_{fw2}$) affects the critical densities ρ_{av1} and ρ_{av2} and the interval $\Delta\rho_{av} = \rho_{av2} - \rho_{av1}$ in which SB occurs.

It was also shown that, at a selected value of ρ_{av}, ϵ_{fw1} and ϵ_{fw2} depend on temperature and the interval $\Delta\epsilon_{fw} = \epsilon_{fw2} - \epsilon_{fw1}$ in which SB occurs decreases with increasing temperature.

The results obtained in the present and previous papers (refs 10 and 11) are based on the assumption that the density distribution is homogeneous in x and y directions. This assumption allowed to reduce the dimensionality of the problem to an one-dimensional one and to obtain numerical solutions which revealed the existence of SB in the h direction. It is, however, possible the closed system to undergo symmetry breaking also in x and y directions through the formation of liquid-like drops on the walls or liquid-like bridges between the walls. Such a possibility was identified in refs 16 and 17 for cylindrical pores in the axial direction. If SB takes place across as well as along the slit simultaneously, then the state with the lowest free energy could be inhomogeneous in all three directions. The complete answer to this question involves the difficult minimization of the free energy with respect to all three coordinates (x, y, h). The results of such calculations should be compared to those obtained in the present paper to verify when the free energy is smaller.

The occurrence of SB in h direction is supported by recent Monte Carlo simulations of argon between parallel identical walls of solid carbon dioxide ($\varepsilon_{fw} = 1.277$), obtained by Errington[18] for a slit with $h^*_m = 20$ at $T = 89.82$ K. In Figure 6, three snapshots representing the equilibrium states of three closed systems are presented for the average densities $\rho^*_{av,1} = 0.123$ (Figure 6a), $\rho^*_{av,2} = 0.246$ (Figure 6b), and $\rho^*_{av,3} = 0.556$ (Figure 6c). (Although oscillations of the density near the wall do exist, they are not visible in these figures.) The critical values ρ^*_{sb1} and ρ^*_{sb2} provided by our theory for these systems are 0.08 and 0.48, respectively, and the density profiles calculated for the average densities used in Monte Carlo simulations are plotted in Figure 7. The states presented in Figure 6a,b belong to the range of average densities where SB should exist according to the present theory (see Figure 7a,b). One of those states (Figure 6a) shows, in agreement with the calculations, an SB in the density distribution across the slit. Another one (Figure 6b) has a density distribution less asymmetrical than the predicted one.

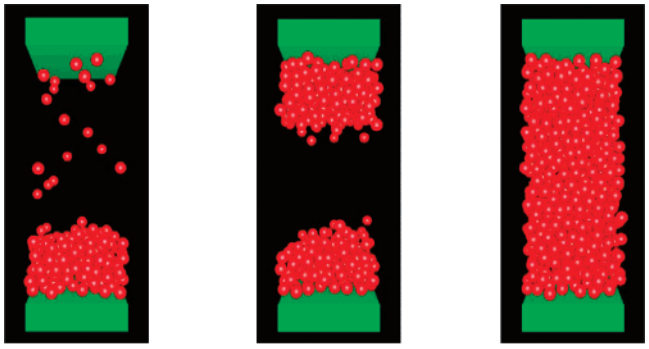

Figure 6. Monte Carlo images of the equilibrium states of argon between walls of solid carbon dioxide ($\varepsilon_{fw} = 1.277$). The width of the slit $h^*_m = 20$ and $T = 89.82$ K. The average densities ρ^*_{av} are (a) 0.123, (b) 0.246, and (c) 0.556.

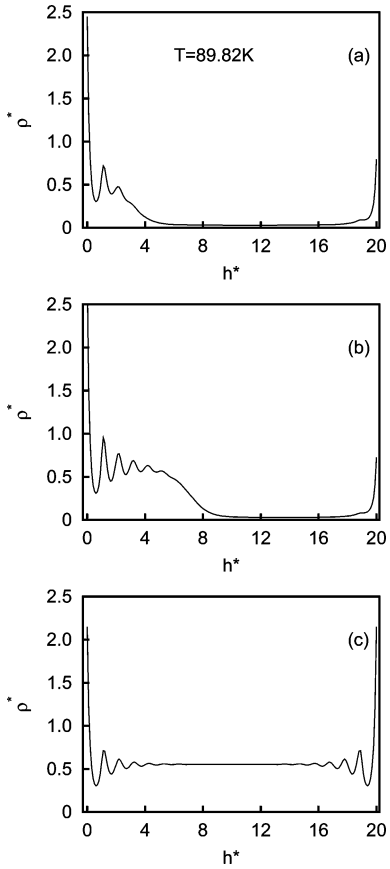

Figure 7. Stable density profiles calculated for argon between walls of solid carbon dioxide ($\varepsilon_{fw} = 1.277$). $h^*_m = 20$, $T = 89.82$ K. The average densities ρ^*_{av} are (a) 0.123, (b) 0.246, and (c) 0.556.

The third (Figure 6c) has a symmetrical distribution corresponding to the average density $\rho^*_{av,3} > \rho^*_{sb2}$, in agreement with the theory (Figure 7c).

Acknowledgment. The authors are grateful to Dr. J. Errington for permission to use the results of his Monte Carlo simulations prior to their publication.

Appendix A

The total fluid-walls interaction $U_s(h)$ in eq 3 is provided by the Lennard-Jones 3−9 potential, obtained by integrating

ϕ_{fw} over the volume of the walls, by assuming constant densities of the walls.[15] This potential has the form

$$U_s(h) = \psi(h) + \psi(h_m - h) \tag{A.1}$$

where

$$\psi(h) = \frac{2\pi}{3}\epsilon_{fw}\rho_w\sigma_{fw}^3\left[\frac{2}{15}\left(\frac{\sigma_{fw}}{\sigma_{fw}+h}\right)^9 - \left(\frac{\sigma_{fw}}{\sigma_{fw}+h}\right)^3\right] \tag{A.2}$$

Taking into account that the density $\rho(\mathbf{r})$ depends only on the distance h, $U_f(h)$ can be written after integration over the lateral coordinates in the form

$$U_f(h) = \int_0^{h_m} dh'\, \rho(h')K(h - h') \tag{A.3}$$

where

$$K(h-h') = 2\pi\epsilon_{ff}\sigma_{ff}^2\begin{cases}\frac{2}{5}\left(\frac{\sigma_{ff}}{h-h'}\right)^{10} - \left(\frac{\sigma_{ff}}{h-h'}\right)^4, & |h-h'| > \sigma_{ff}, \quad \text{(A. 4)}\\ -\frac{3}{5}, & |h-h'| \le \sigma_{ff} \quad \text{(A. 5)}\end{cases}$$

The derivative $(\partial\Delta\Psi_{hs}[\bar{\rho}(h')]/\partial\bar{\rho}(h'))$ in eq 5 is given by

$$\frac{\partial\Delta\Psi_{hs}[\bar{\rho}(h')]}{\partial\bar{\rho}(h')} = k_BT\frac{\pi}{6}\sigma_{ff}{}^3\frac{4-2\eta_{\bar{\rho}}}{(1-\eta_{\bar{\rho}})^2}, \quad \eta_{\bar{\rho}} = \frac{\pi}{6}\bar{\rho}(h')\sigma_{ff}{}^3 \tag{A.6}$$

Appendix B

Using eq 1 for the Helmholtz free energy, one obtains the following expression for the second variation δ^2F with respect to small perturbations $\delta\rho^*(z)$ and $\delta\rho^*(z')$:

$$\frac{\delta^2F}{k_BT/\sigma_{ff}{}^2} = \int_0^{z_m}\frac{dz}{\rho^*(z)}\delta\rho^*(z) + \int_0^{z_m} dz\, \delta\rho^*(z)\int_0^{z_m} dz'\, X(z, z')\delta\rho^*(z') \tag{B.1}$$

where the dimensionless variable z stands for h/σ_{ff} and $\rho^*(z) = \rho(z)\sigma_{ff}{}^3$. In eq B.1

$$X(z, z') = f_0[\bar{\rho}^*(z)]\varphi_1(z, z') + K_1(z - z') + 2\pi\sum_{k=0}^{2}X_k(z, z') \tag{B.2}$$

where

$$X_k(z, z') = \frac{1}{\alpha(z')}f_k[\bar{\rho}^*(z')]J_k(z - z') + \int_0^{h_m} dz''\, \frac{\rho(z'')}{\alpha(z'')}\frac{\partial f_k[\bar{\rho}^*(z'')]}{\partial\bar{\rho}^*(z'')}J_k(z - z'')\varphi_1(z'', z') - \int_0^{h_m} dz''\, \frac{\rho(z'')}{\alpha^2(z'')}f_k[\bar{\rho}^*(z'')]J_k(z - z'')\varphi_2(z'', z') \tag{B.3}$$

$$\alpha(z) = 1 - \bar{\rho}_1{}^*(z) - 2\bar{\rho}^*(z)\bar{\rho}_2^*(z) \tag{B.4}$$

$$f_k[\bar{\rho}^*(z)] = \frac{\pi}{6}\frac{4 - \frac{\pi}{3}\bar{\rho}^*(z)}{\left[1 - \frac{\pi}{6}\bar{\rho}^*(z)\right]^3}[\bar{\rho}^*(z)]^k \tag{B.5}$$

$$\varphi_1(z, z') = 2\pi\sum_{k=0}^{2}\frac{\partial\bar{\rho}^*(z)}{\partial\bar{\rho}_k^*(z)}J_k(z - z') \tag{B.6}$$

with

$$\varphi_2(z, z') = -2\pi[J_1(z - z') + 2\bar{\rho}^*(z)J_2(z - z')] - 2\bar{\rho}_2^*(z)\varphi_1(z, z') \tag{B.7}$$

$$K_1(z - z') = \frac{2\pi\epsilon_{ff}}{k_BT}\begin{cases}\frac{2}{5}\left(\frac{1}{z-z'}\right)^{10} - \left(\frac{1}{z-z'}\right)^4, & |z - z'| > 1,\\ -\frac{3}{5}, & |z - z'| \le 1\end{cases}$$

$$J_0(z - z') = \begin{cases}\frac{3}{8\pi}[1 - (z - z')^2], & |z - z'| \le 1,\\ 0, & |z - z'| > 1\end{cases}$$

$$J_1(z - z') = \begin{cases}A - \frac{a_0}{2}(z - z') - \frac{b_1}{3}|z - z'|^3 - \frac{b_2}{4}(z - z')^4, & |z - z'| \le 1,\\ B - d_1|h - h'| - \frac{c_0}{2}(z - z')^2 - \frac{m_1}{3}|z - z'|^3 - \frac{m_2}{4}(z - z')^4, & 1 < |z - z'| \le 2,\\ 0, & |z - z'| > 2\end{cases}$$

$$J_2(z - z') = \begin{cases}\frac{5\pi}{144}\left[1 - 3(z - z')^2 + 4\left|z - z'\right|^3 - \frac{5}{4}(z - z')^4\right], & |z - z'| \le 1,\\ 0, & |z - z'| > 1\end{cases}$$

In the above expressions $a_0 = 0.475$, $b_1 = -0.648$, $b_2 = 0.113$, $c_0 = -0.924$, $d_1 = 0.288$, $m_1 = 0.764$, $m_2 = -0.187$, $A = (1/2)a_0 + (1/3)b_1 + (1/4)b_2 + d_1 + (3/2)c_0 + (7/3)m_1 + (15/4)m_2$, and $B = 2d_1 + 2c_0 + (8/3)m_1 + 4m_2$.

References and Notes

(1) Tarazona, P.; Marconi, U. M. B.; Evans, R. *Mol. Phys.* **1987**, *60*, 573.
(2) Magda, J. J.; Tirrel, M.; Davis, H. T. *J. Chem. Phys.* **1985**, *83*, 1888.
(3) Evans, R.; Marconi, U. M. B.; Tarazona, P. *J. Chem. Phys.* **1986**, *84*, 2376.
(4) Evans, R. *J. Phys.: Condens. Matter* **1990**, *2*, 8989.
(5) Sarman, S. *J. Chem. Phys.* **1990**, *92*, 4447.
(6) Lastoskie, C.; Gubbins, K. E.; Quirke, N. *Langmuir* **1993**, *9*, 2693.
(7) Maciolek, A.; Evans, R.; Wilding, N. B. *J. Chem. Phys.* **2003**, *119*, 8663.
(8) Löwen, H. *Phys. Rep.* **1994**, *237*, 249.
(9) Merkel, M.; Löwen, H. *Phys. Rev. E* **1996**, *54*, 6623.
(10) Berim, G. O.; Ruckenstein, E. *J. Phys. Chem. B* **2007**, *111*, 2514.
(11) Berim, G. O.; Ruckenstein, E. *J. Chem. Phys.* **2007**, *126*, N 124503.
(12) Nilson, R. H.; Griffiths, S. K. *J. Chem. Phys.* **1999**, *111*, 4281.
(13) Tarazona, P. *Phys. Rev. A* **1985**, *31*, 2672.
(14) Evans, R.; Tarazona, P. *Phys. Rev. A* **1983**, *28*, 1864.
(15) Ebner, C.; Saam, W. F. *Phys. Rev. Lett.* **1977**, *38*, 1486.
(16) Vishnyakov, A.; Neimark, A. V. *J. Chem. Phys.* **2003**, *119*, 9755.
(17) Ustinov, E. A.; Do, D. D. *J. Chem. Phys.* **2004**, *120*, 9769.
(18) Errington, J. Personal communication.